Shape- Based Tracking and Analysis of Myocardial Function from 4D Images

J. S. Duncan, P. Shi, A. Amini, T. Constable, and A. Sinusas
Departments of Diagnostic Radiology, Medicine, and Electrical Engineering
Yale University
New Haven, CT 06520

Abstract

This paper is a status report of work- in- progress, unded by the National Heart, Lung and Blood Institute NHLBI) of the National Institutes of Health (NIH), hat is aimed at more accurately and objectively deter- ining and quantifying the regional and global function f the left ventricle (LV) of the heart under both nor- al and ischemic conditions, fundamentally relying on omputer vision- like models and strategies.

1 Introduction

he quantification of left ventricular (LV) regional func- on from diagnostic images permits clinically important easurements to be made that are crucial for manag- g patients with ischemic heart disease. However, such easurements have been hampered by limitations in nventional imaging and image analysis methodology at have commonly been applied in the clinical arena date. These limitations have prohibited the accu- te regional assessment of myocardial injury and/or the rediction of vessel patency, and include the facts that:) most conventional imaging methods provide two- imensional (2D) temporal slice or projection sequences .g. see [4]), that cannot possibly permit viewing or alysis of the true motion of the heart, which rigidly oves and non- rigidly deforms in a three- dimensional D) space. 2.) Most approaches to regional image- ased analysis of LV function : a.) make gross and re- rictive assumptions about the general direction of LV otion or thickening (e.g. towards a center of mass-]) and b.) utilize only the end diastolic (ED) and end- stolic (ES) image frames (e.g. [3]), ignoring the fact at the LV actually goes through a temporal wave of ntraction and that the asynchrony of surface motion LV thickening from region to region may be indicative ischemia.

Our current research utilizes techniques from com- ter vision to analyze 3D cardiac image sequences in der to more accurately estimate regional LV function, d is much more adaptable to the nonlinear, non- rigid gional motion of the LV than the techniques based on the restrictive assumptions mentioned above. The approach is based on the use of non-invasive, three-dimensional (3D), cardiac diagnostic imaging sequences (i.e. four-dimensional (4D) data) acquired from any one of a number of modalities- currently 3D cine Computed Tomography (CT) acquired from the Dynamic Spatial Reconstructor (DSR) at the Mayo Clinic and cardiac Magnetic Resonance Image (MRI) data acquired at our own facility and soon to be tested on 3D transesophogeal echocardiographic data. Our image analysis methodology follows the shape properties of the endocardial and epicardial surfaces of the LV over the entire cardiac cycle, based on locating and matching differential geometric landmark features and using a mathemetical optimization reasoning strategy to combine smoothness models with data- derived information. In some respects, this approach has similar goals as other recent efforts in the medical imaging community that utilize the unique characteristics of MR imaging techniques to track cardiac wall motion and function: MR tagging (e.g. [2]) and phase- contrast velocity imaging ([6]). It is of interest to note that the shape- based approach can derive quantitative parameters of LV function similar to those derived from these MRI- based approaches, yet is not restricted to using only MRI data.

2 Image Analysis Methods

Surface segmentation. The 4D image datasets are first segmented by treating the data as if it consisted of a sequence of temporal frames where there exists a spatial stack of 2D images in each frame. We solve the 2D boundary finding problem twice in each image, once for the epicardial border and once for the endocardial border using a deformable contour approach that we have developed for 2D boundary finding [7]. The boundaries found in this plane are now used as a bias and initial estimate for locating the endocardial and epicardial boundaries in the next plane in the stack. This process repeats until all of the contours that make up the LV surfaces in each frame are completely located. Finally, the contours that form the endocardial and epicardial surface in each 3D frame are stacked and then sent to a surface

Figure 1: Gray scale renderings of color- coded bending energy maps of four, temporally- consecutive endocardial surfaces of the dog heart in its normal, or baseline, state. The sequence progresses as follows: upper left, upper right, lower left, lower right.

tesselation algorithm that we have implemented, which typically creates roughly 15,000 triangles per DSR- derived endocardial surface and 3,000 triangles per MRI-derived endocardial surface.

Shape- based motion tracking. As mentioned above, the movement over time of a set of LV surface points is performed by following local surface shape. Our approach reflects further developments, improvements and modifications to our earlier efforts in this area [1]. The dense set of points found from tesselating the surfaces are used to guide shape calculations. Between any 2 surfaces, shape matching is first performed through the use of a metric based on comparing surface patches using bending energy. The basic idea is to match a surface patch on a 3D (endocardial or epicardial) surface found from an image frame at time t with a surface patch within a region of surface patches on a corresponding 3D surface found from an image frame at time $t + \delta t$, using measurements of the patches' mean and Gaussian curvatures. We model the surface patches as elastic thin-plates, where the energy needed to bend each plate away from any arbitrarily formed initial surface to a deformed state is

$$\epsilon_{be}(u,v) = \left\{ \left[\frac{\kappa_1^2(u,v) + \kappa_2^2(u,v)}{2} \right]^{\frac{1}{2}} - \left[\frac{\bar{\kappa}_1^2(\bar{u},\bar{v}) + \bar{\kappa}_2^2(\bar{u},\bar{v})}{2} \right]^{\frac{1}{2}} \right\}^2 \quad (1)$$

The principal curvatures of a surface patch at time t_0 are given with no bars, while the same parameters at time $t_0 + \delta t$ (within a search window on the second surface) are specified with bars. This equation arrives at a numerical value measuring the energy that was required to deform the surface patch surrounding surface point (u, v) at time t_0 to achieve a particular shape at a test position within a search window at time $t_0 + \delta t$. Each of the $\frac{\kappa_1(u,v)^2 + \kappa_2(u,v)^2}{2}$ terms in this equation can separately be seen as computing the amount of bending energy required to bend a thin, flexible, flat plate to the shape of the surface patch surrounding point (u, v). Pseudocolor maps of the local bending energies can be displayed on top of surface renderings of the LV. A gray scale display of such mappings/ renderings is shown in figure 1 for four sequential endocardial surfaces, reconstructed from a MRI 4D acquisition. The result of the matching process specified by equation (1) essentially compares the maps displayed in figure 1 and yields a set of initial shape- based, best- match vectors, $\mathbf{D}_0(u, v)$, for pairs of surfaces derived from the 4D image sequence, as well as information about the uniqueness of the match within each search region. This information is now sent to a regularizing functional that will include terms to smooth over (u,v) surface space:

$$\mathbf{D}^*(\mathrm{u,v}) = \arg\min_{\mathbf{D}} \int_U \int_V C_{\mathbf{D}}(\mathrm{u,v})[\mathbf{D}(\mathrm{u,v}) - \mathbf{D_0}(\mathrm{u,v}) + \frac{\partial \mathbf{D}(\mathrm{u,v})}{\partial \mathbf{u}}] \, d\mathbf{u}$$

In this equation, U, V is the domain of the surface at time t in which the finite element grid from the Delaunay triangulation is embedded, $\mathbf{u} = [uv]^T$ is the position of the end of the vector $\mathbf{D}(u, v)$ on the surface found at time t, $\mathbf{D}^*$ (u,v) is the optimal smoothed motion vector field between any two surfaces found at times t and $t + \delta t$, $\mathbf{D_0}$ (u,v) is the initial motion vector estimate, and $C_{\mathbf{D}}$ (u,v) is the confidence measure matrix from the initial estimation, which weights the overall goodness of the initial match as well as the match uniqueness within the search area. While this model currently serves as a spatial smoothness model for the vector field, the bulk of our current efforts are aimed at incorporating appropriate temporal models as well. The solution of this functional will yield a set of smoothed flow vectors that better estimate true local LV motion. It should be clear that ultimately strong, unique matches, according to the bending energy match measure, that last over several frames, are weighted via the confidence measures to be the most influential shape- based landmarks. Flow vectors running through the knot points of the surface patches are connected in order to form trajectories that track individual points' motion over the entire cardiac cycle. The current strategy is to estimate and track the trajectories of motion of a dense field of points that sample the LV endocardial and epicardial surfaces at 1 point in time, over the entire cardiac cycle. The results

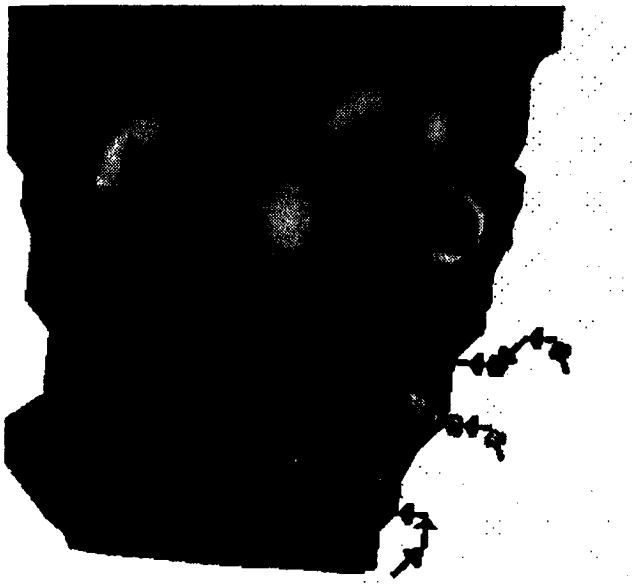

'igure 2: Algorithm- computed trajectories of several ndocardial points for the normal or baseline heart. The rajectories begin at the end- diastolic surface and end t the end- systolic surface (rendered here).

f computing several of these trajectories in the antero-pical region of the heart from MRI- derived endocardial urfaces, are shown in figure 2. LV motion and function ıdices are then derived from these trajectories, and in-lude i.) the sum of the magnitudes (lengths) of the flow ectors, or path length $L_{path,\alpha}(h,i)$, ii.) the shape of ıe path (compared to a linear trajectory), $s_{path,\alpha}(h,i)$ nd iii.) the peak velocity within the path, $v_{peak,\alpha}(h,i)$. ach of these measures are recorded for each trajectory, ıdexed by i, on each heart being studied, indexed by h. ı general, these trajectories will be used to create quan-tative measures of endocardial surface motion and LV ıickening/ strain.

3 Experiments and Results

'he methodology is currently being validated using ɔmputer simulations of linearly deformable objects and nage data acquired from acute dog studies. The acute ogs will have image-distinguishable markers (radio-paque wires for cine CT and a combination of copper lugs (endocardium) and a gadolinium/ water mixture-lled pellet (epicardium) for MRI) sewn to the LV wall. Images from 3 slices of a single 3D frame from a 4D IRI acquisition are shown in figure 3. The arrows point ɔ the markers (dark voids on the endocardium and right spots on the epicardium). The validation test-ıg is being performed utilizing data from 5 studies ac-uired from each of two different imaging modalities (i.e. ıe current test set consists of ten 4D data sets): 4D ated/cine Magnetic Resonance Imaging and 4D real-time cine Computed Tomographic Imaging (using data from the Dynamic Spatial Reconstructor). Table 1 illustrates the comparison of bending energy-derived measures from an infarcted heart derived from DSR image data to the same measures derived from the manually tracked movement of four implanted endocardial markers (i.e. the gold standard) derived from the same images. These comparisons were made using only the raw, unsmoothed curvedness vectors $\mathbf{D_0}(u,v)$ to perform the matching from which the algorithm- based trajectories were derived.

Ultimately, our goal is to better distinguish and characterize the spatial/ temporal extent and function of regions of ischemia and infarction in the LV wall, as well as gain insight into LV post- MI remodeling. Thus, further studies are underway to compare these algorithm-derived *in vivo* measures to measures of *post mortem* injury. By studying a spatially dense set of points that sample the LV wall's surfaces over many temporal frames within a cardiac cycle and over a range of conditions of LV wall abnormality, we will be able to better understand the regional and global physiological processes associated with ischemic heart disease.

4 Summary

In the workshop presentation of this paper, we have described a shape- based LV motion tracking algorithm, the image data we are using, and the graphical methods being used to visualize the results. In addition, we have presented initial qualitative and quantitative data aimed at comparing the algorithm- derived motion trajectories to those found using implanted marker gold standards. Further methodology work continues along the lines of developing improved temporal models for motion tracking, including incorporating additional differential geometric features into the matching algorithm and forming more complete 4D visualization approaches. Validation and clinical experimentation continues based on the *in vivo* acute infarct models and using DSR and MR image data.

Acknowledgements

The authors would like to thank Dr. Erik Ritman for the DSR data from which the results in Table 1 were computed, and Drs. F. Lee and T. McCauley, for earlier discussions. This work was funded by NIH-NHLBI grant R0144803.

References

[1] A. A. Amini and J. S. Duncan. Bending and stretching models for lv wall motion analysis from curves and surfaces. *Image and Vision Computing*, 10(6):418–430, 1992.

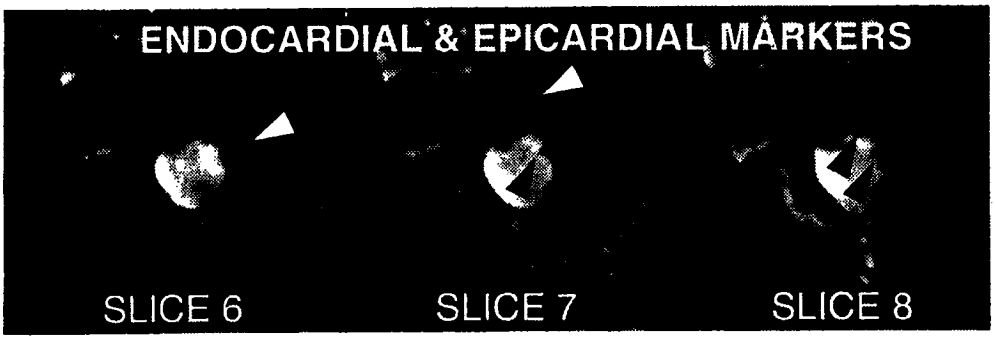

Figure 3: Three slices from the same 3D MRI time frame, illustrating the paired markers used for motion tracking validation (white arrows= epicardial markers, black= endocardial markers).

	path length			displacement length		
Marker no.	$L_{path,\mathbf{gold}}$	$L_{path,\mathbf{alg}}$	δ_{path}	$L_{disp,\mathbf{gold}}$	$L_{disp,\mathbf{alg}}$	δ_{disp}
1	30.48	29.77	0.71	12.02	15.44	3.42
2	36.38	25.28	11.10	17.47	15.27	2.20
3	23.89	31.65	7.76	13.64	12.02	1.62
4	32.15	26.48	5.67	12.42	12.44	0.02
μ_δ			6.31mm			1.81mm
σ_δ			3.77mm			1.22mm

Table 1: Table of path lengths ($L_{path,\alpha}$) and complete path displacements ($L_{disp,\alpha}$) at four endocardial marker positions of a single heart. These data were computed using 1mm^3 4D DSR image data, and compare algorithm-computed trajectories ($\alpha = alg$) to the trajectories of implanted markers ($\alpha = gold$). Note that μ_δ and σ_δ represent the means and standard deviations of the differences in the measurements.

[2] L. Axel and L. Dougherty. MR imaging of motion with spatial modulation of magnetization. *Radiology*, 171:841–845, 1989.

[3] E. L. Bolson, S. Kliman, F. Sheehan, and H. T. Dodge. Left ventricular segmental wall motion - A new method using local direction information. In *Proc. of Computers in Cardiology*, 1980.

[4] S. Collins and D. Skorton. *Cardiac Imaging and Image Processing*. McGraw Hill, New York, 1986.

[5] D. Zisserman et al. Cardiac catheterization and angiographic analysis computer applications. *Progress in Cardiovascular Diseases*, XXV:409–434, 1983.

[6] N. J. Pelc, A. Shimakawa, and G. H. Glover. Phase contrast cine MRI. In *Proceedings of the 8th Annual SMRM*, page 101, Amsterdam, 1989.

[7] L. Staib and J. S. Duncan. Parametrically deformable contour models. *IEEE Trans. on Patt. Anal. and Mach. Intell.*, 14(11):1061–1075, 1992.